Quantifying Local to Regional Emissions of Methane Using UAV-based Atmospheric Concentration Measurements

Andersen, Truls

DOI:
10.33612/diss.190478126

CHAPTER 1

Introduction

1.1 Climate

Changes are and have always been a part of our planet. Since the early years of the Earth, our world has gone from having almost no atmosphere to having an atmosphere dominated by volcanic compounds and finally arriving at the nitrogen- and oxygen-rich atmosphere we know and breathe today (Pavlov et al., 2000). Since the last glaciation 11700 years ago to around the 1700s, the atmospheric composition has remained relatively unchanged. Fast forward to modern times, and we see a very different picture. In recent times the atmosphere has seen change at exceedingly higher rates than previously observed. These changes can largely be attributed to increased human activity and are known as anthropogenic changes. The human race has existed for about 200.000 years and has, throughout its existence, influenced local changes to the environment. In recent times, the anthropogenic influence is no longer limited to only local scale environmental changes but global.

For the most part, the global temperature is dependent on the incoming solar radiation. The Earth absorbs the radiation but is also irradiating back towards space. If we consider Earth without atmosphere, the average temperature would be close to -17 [°C], far below that of the actual value. The atmosphere that surrounds our globe consists of a multitude of greenhouse gases such as water vapor (H_2O), carbon dioxide (CO_2), methane (CH_4), and nitrous oxide (N_2O). These gases have the ability to both absorb and emit infrared radiation. As the sun irradiates the planet, the short-wave solar radiation is absorbed and starts heating the surface. As the surface is heated, energy is re-emitted back into the atmosphere via longwave radiation. The greenhouse gases that are part of our atmosphere absorb some of this energy and pass along excess kinetic energy to surrounding molecules, such as O_2 and N_2, which re-emit the radiation back towards the surface, effectively causing energy to be trapped within the atmosphere. The accumulation of heat within

our atmosphere is why our globe does not have a mean temperature of -17 [°C] but instead sits at a more comfortable mean surface temperature of around 15 [°C]. If it was not for our atmosphere and its greenhouse gas components, our world would look drastically different than it does today (Kump et al., 2009; Marshall and Plump, 2008).

1.1.1 Modern climate change

One of the significant issues we see and hear about today is increasing global warming. As previously mentioned, the atmosphere and greenhouse effect play a vital role in regulating the temperature of our globe. The industrial revolution began in the 1750s, and since then, anthropogenic emissions have increased dramatically. These emissions come from many different aspects of our society, like deforestation and fossil fuel burning. These activities have led to increased emissions of CO_2, CH_4, and other greenhouse gases to the atmosphere, which has led to changes in the atmospheric composition. With the climate remaining fairly constant since the last glaciation up until the industrialization, it is undeniable that human-made activities have caused the dramatic changes seen over the last decades (Dessler, 2015). The global mean temperature is an example of this, which from 1880 to 2018, increased by ~ 0.87 [°C] (Shukla et al., 2019). This is shown in figure (1.1) **a**.

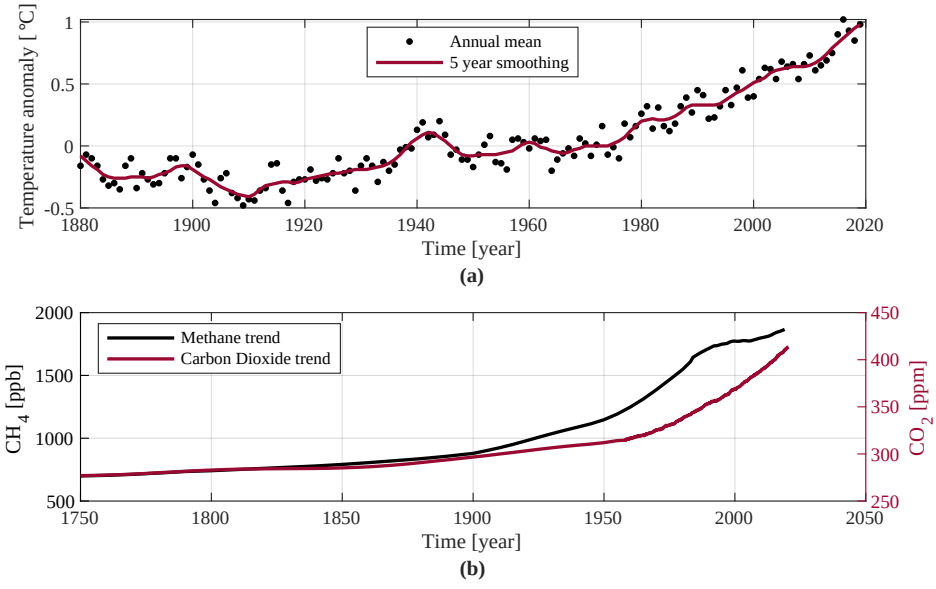

Figure 1.1. **(a)** shows how the global mean temperature has changed over the past 139 years. The data is from the National Aeronautics and Space Administration (NASA) (NASA, 2020). **(b)** shows the CO_2 and CH_4 trends from 1750 to 2019. The CO_2 is taken from Etheridge et al. (1998a) and Dlugokencky et al. (2020), and the CH_4 data is taken from Etheridge et al. (1998b) and Dlugokencky (2020).

The most abundant anthropogenic greenhouse gas is CO_2 (Kump et al., 2009). Mole fractions of atmospheric CO_2 have varied by only 20 parts per million (ppm) over the last 8000 years before the industrialization, where the variations likely stem from natural

causes, like volcanic eruptions. Since the 1700s, and the beginning of the industrial revolution, CO_2 mole fraction levels have risen by more than 100 [ppm] (Etheridge et al., 1998a; Dlugokencky et al., 2020). Figure (1.1) **b** shows the increasing mole fraction levels of CO_2 and CH_4, two of the most important and impactful anthropogenic greenhouse gases. The impact a specific greenhouse gas has on our climate is often explained through radiative forcing. Radiative forcing is defined as the net difference between incoming solar energy that the Earth absorb and the energy that is radiating back towards space. A positive radiative forcing implies that more energy is absorbed than emitted, thus yielding in a warming effect, and likewise, a negative radiative forcing implies a larger emission of energy, causing a cooling effect (IPCC, 2013). Understanding the mechanisms behind what drives these greenhouse gases is vital to developing new and accurate ways to predict how our climate is changing. Quantification of the atmospheric composition is a crucial tool to reach that goal. The greenhouse gas of focus during this thesis will be CH_4.

1.2 The global methane cycle

Methane is the second most abundant long-lived anthropogenic greenhouse gas, only trumped by carbon dioxide. Over the last 650000 years, atmospheric methane concentration has fluctuated between 350 - 800 parts per billion (ppb) (Loulergue et al., 2008). Since preindustrial times, the mole fraction of methane has increased by approximately 2.6 times, measuring in at a global mean of 1873.7 [ppb] in 2020 (Dlugokencky, 2020). As mentioned in the previous section, this increase is primarily attributed to increased anthropogenic emissions. These emissions arise mainly from fossil fuel production and use, agriculture, biomass burning, and waste management. Increased atmospheric CO_2 mole fractions alongside rising global temperatures also change the emission of natural CH_4 sources, further increasing the anthropogenic emitted CH_4 indirectly (IPCC, 2013). Although the abundance of CH_4 is smaller than that of CO_2, it has a warming potential 28 times greater over a 100 year time period (Etminan et al., 2016; Van Dingenen et al., 2018). In the period 2003 - 2012, the emitted methane to the atmosphere was estimated to be 558 [Tg CH_4 yr^{-1}] (Saunois et al., 2016a,b; Global Carbon Project, 2016). The methane emissions to the atmosphere and methane sinks are shown in figure (1.2). The global anthropogenic CH_4 emissions are estimated around 366 [Tg CH_4 yr^{-1}] (Saunois et al., 2016a), which represents 3 [%] of the global CO_2 anthropogenic emissions in terms of carbon mass flux. Despite this small percentage, the increasing CH_4 mole fractions have contributed to $\sim$ 23 [%] ($\sim$ 0.62 [W m^{-2}]) to the additional radiative forcing accumulated in the lower atmosphere since preindustrial times (Etminan et al., 2016). The lifetime of CH_4 in the atmosphere ranges from 8.4 to 12 years (Ehhalt et al., 2001), due to influence from other chemical compounds like nitrogen oxides (NO_x) or CO_2, and the changing lifetime therefore changes the effective radiative forcing that CH_4 contributes. Methane is in itself contributing to the production of other chemical compounds in the atmosphere, like ozone (O_3), stratospheric water vapor (H_2O), and CO_2. It also, and perhaps more importantly, affects its own lifetime through chemical reactions with hydroxyl radical (OH) molecules in the atmosphere, which increases or decreases the contribution that CH_4 has on the radiative forcing. Effectively, the total radiative forcing attributable

to anthropogenic CH_4 emissions are 0.97 [W m^{-2}] (Myhre et al., 2013). Due to the indirect effects of CH_4 on its own lifetime and its interaction with other atmospheric species, stabilization or reduction of CH_4 emissions leads to a stabilization or reduction of its atmospheric concentration, and in turn, radiative forcing (Saunois et al., 2020). Therefore, reducing methane emissions is recognized, especially on shorter, decadal timescales, as an effective option for climate change mitigation (Shindell et al., 2012).

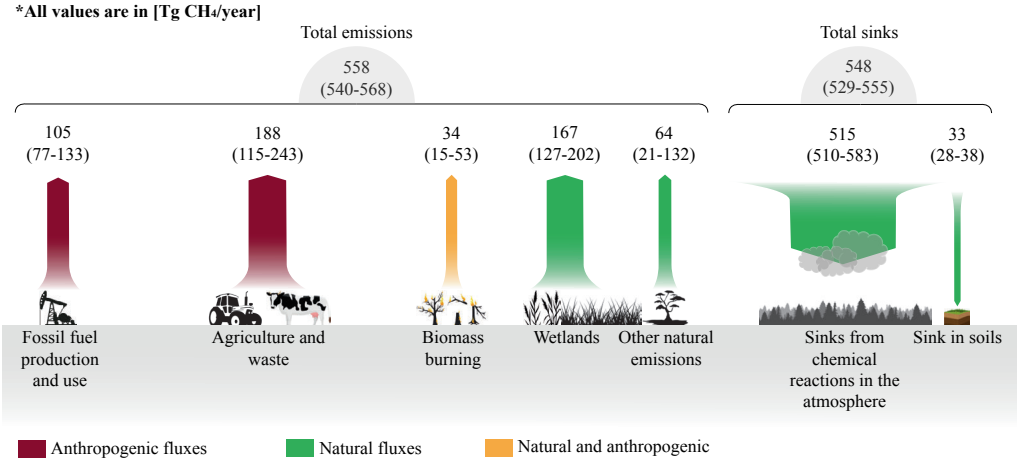

Figure 1.2. shows the CH_4 inventory balance for the year 2003 - 2012. This figure is a re-illustration of the originally posted figure by Global Carbon Project (2016), where the data comes from Saunois et al. (2016a) and Saunois et al. (2016b).

According to Kirschke et al. (2013), Saunois et al. (2017), and Turner et al. (2019), over the past decades, changes in the magnitude of methane sources and sinks are characterized by high uncertainties. Anthropogenic emissions are reported with relative uncertainties of 20 - 35 [%] from sectors such as fossil fuels and agriculture, and about 50 [%] from biomass burning and natural wetlands. Relative uncertainties reach up to and above 100 [%] for a wide range of other natural sources, like inland water or geological sources (Saunois et al., 2020).

1.2.1 Sources and sinks

Methane emissions can be broadly grouped into three separate categories: Biogenic, thermogenic, and pyrogenic emissions. Biogenic sources contain methane generating microbes, referred to as methanogens and occurs in anaerobic environments (Environments that lack oxygen). Examples of anaerobic environments are natural wetlands, rice paddies, oxygen-depleted- or starved freshwater reservoirs (like dams), digestive systems of ruminants and termites, and organic waste deposits (i.e., manure, sewage, and landfills) (Kirschke et al., 2013). Thermogenic methane is a fossil fuel. That means it was formed through geological processes over extended time frames, typically millions of years. One way thermogenic methane enters the atmosphere is via natural features that vent the methane from beneath the surface directly into the atmosphere. Thermogenic methane can originate from mud volcanoes, terrestrial seeps, or marine seeps. The use and exploitation of fossil fuels like coal, oil, and natural gas also release thermogenic methane into the atmosphere. Lastly,

we have pyrogenic methane sources, where methane is generated via incomplete combustion of biomass- and soil-carbon during wildfires, biofuels, and fossil fuels (Kirschke et al., 2013).

The main sink for atmospheric methane is the chemical reaction between methane and radicals, primarily hydroxyl radicals (OH), which occurs predominantly within the troposphere. Hydroxyl radicals are negatively charged and bond with methane via a series of chemical chains, ultimately producing CO, and then CO_2 (Jacob, 1999). Methane that passes through the troposphere and into the stratosphere face the same chemical reactions along with two additional reactions; with chlorine (Cl) and oxygen (O^1D). The OH radicals typically have very short lifetimes ($\sim$ 1 [s]), which leads to difficulties obtaining proper measurements of its abundance. Difficulties in accurately measuring OH in the atmosphere therefore create more uncertainty on how much CH_4 is being scrubbed from the atmosphere.

1.2.2 Isotopic signature

Information about which emission source the atmospheric methane originated from can often be discovered through isotopic signatures. Methane consists of a single carbon atom and four hydrogen (H) atoms. However, different sources and sinks of methane can have a distinct affinity for the selected isotopes (^{12}C & ^{13}C, and H & ^{2}H). The deviation from the ratio between stable isotopes is denoted by using δ, and taking ^{12}C and ^{13}C as an example, is calculated as:

$$\delta^{13}C_{sample} = \left(\frac{^{13}C/^{12}C_{sample}}{^{13}C/^{12}C_{standard}} - 1 \right) \cdot 1000 \text{ ‰} \tag{1.1}$$

As mentioned, biogenic, thermogenic, and pyrogenic sources all have unique δ^{13}C-CH_4 and δ^{2}H-CH_4 Hence, isotopic composition measurements can distinguish between different methane sources (Kirschke et al., 2013). These isotope ratios can vary significantly from each other (Schwietzke et al., 2016). However, attributing isotopic signatures to atmospheric emitters is only possible if the isotopic signatures are shown to be coherent across specific source categories (Fisher et al., 2017). This is not trivial, as there are often extensive temporal variations within each source category and variations depending on the emission's geographic location (Zazzeri et al., 2016). For the work done during this thesis, isotopic measurements were made from coal mine ventilation shafts, to identify whether the methane originated from that source. This is part of the work of chapter 4.

1.3 The Upper Silesia Coal Basin

The Upper Silesia Coal Basin (USBC) in southern Poland is the location of more than 60 sites related to black coal mining operations, both open-air mines and ventilation shafts connected to underground mining tunnels. The locations of these sites are shown in figure (1.3). The process of extracting coal from the bedrock releases large amounts of methane and to avoid that the air becomes toxic for the working miners, the released methane

is vented to the atmosphere through ventilation shafts located on the surface (see upper right picture of figure (1.3)). The USBC reportedly contributed to 447 [kT] of emitted methane in 2017 (E-PRTR, 2017), making it a strong contributor to Europe's total annual methane emission, however, there is much uncertainty in this estimate. It is therefore an important region to study and quantify methane emissions, which is why this thesis will be focusing on this region.

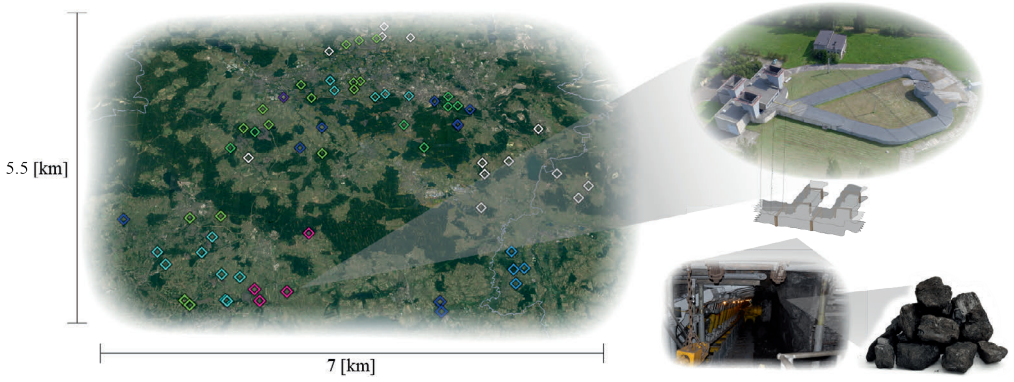

Figure 1.3. shows the location of coal mining sites in the Upper Silesia Coal Basin, Poland, in a area of about 40 [km^2] (left). Figures of a coal mine ventilation shaft (upper right), along with a mining tunnel (middle bottom) and a pile of anthracite coal (bottom right).

1.4 Understanding the methane budget

1.4.1 Global

To track and predict the atmospheric concentration of methane worldwide, it is crucial to have high-quality global measurements. One organization that facilitates global coverage and measurements of CH_4 is the World Meteorological Organization (WMO). They provide the framework for an observational network measuring greenhouse gases around the globe, including atmospheric, land- and ocean-based measurements. As part of WMO's purpose, besides establishing networks of climate observation, they want to create observational standards that are used worldwide. This is to ensure the homogeneity of statistics and data by employing the same practices and procedures all over the world (WMO, 2020b). The WMO network consists of over 10000 surface weather stations, both automatic and crewed, about a 1000 upper-air stations, 700 ships, 100 moored and 1000 drifting buoys, several hundred weather radars, and about 3000 specially equipped commercial aircraft (WMO, 2020a). However, observations of CH_4 are only one of the many interests the WMO has, as the global network covers other meteorological, hydrological, and other geophysical observations as well. On top of the many stations, aircraft, buoys, and ships listed above, the WMO network also includes about 30 meteorological satellites and 200 research satellites, to give full global coverage. Another global greenhouse gas monitoring network that focuses on measurements of CO_2, CH_4, CO, N_2O, and other trace gases, is the Total Carbon Column Observing Network (TCCON). The TCCON network primarily uses Fourier transform spectrometers on their sites, which measures absorbed

direct sunlight from trace gases in the atmosphere, predominantly in the near-infrared. This technique provides a measurement of the total column abundance for the previously mentioned trace gases. Due to these measurements' nature, the TCCON network provides independent measurements to which satellites can be validated over TCCON sites around the globe (TCCON, 2020).

Methane satellite coverage

The first satellite to measure atmospheric CH_4 with sensitivity down to the earth's surface was the European Space Agency (ESA) operated ENVIronmental SATellite (ENVISAT), which housed the Scanning Imaging Absorption Spectrometer for Atmospheric Cartography (SCIAMACHY) (Bovensmann et al., 1999). It could measure tropospheric concentrations of O_3, O_2, O_4, NO_2, N_2O, CO, CO_2, CH_4 and H_2O. It was launched in May 2002, and its mission ended 10 years later in May 2012. During its operation, it reached global coverage in 6 days, and achieved a spatial resolution of 60×30 [km] (Frankenberg et al., 2005). Bergamaschi et al. (2013) used SCIAMACHY satellite retrievals, together with National Oceanic and Atmospheric Administration (NOAA) surface measurements to inversely model atmospheric methane concentrations during 2003 to 2010. After the end of ENVISAT's mission, only one satellite measuring atmospheric CH_4 with near-surface sensitivity remained. This was the Greenhouse gases Observing SATellite (GOSAT), a satellite launched in January 2009. On-board sits the Thermal and Near Infrared Sensor for Carbon Observation Fourier-Transform Spectrometer (TANSO-FTS), which detects gas absorption spectra of the solar short wave infrared (SWIR) reflected on the Earth's surface as well as of the thermal infrared radiated from the ground and the atmosphere (Kuze et al., 2009). GOSAT detects CO_2, CH_4, O_3, H_2O, and can reach global coverage in about 3 days, with spatial resolutions of 10 [km] in diameter. In October 2017, a satellite named the Sentinel 5 Precursor was launched, and on-board was an instrument called the TROPOspheric Monitoring Instrument (TROPOMI). This instrument measures reflected sunlight in the ultraviolet, visible, near-infrared, and shortwave infrared spectral range. This allows for the global coverage of atmospheric species, such as O_3, NO_2, SO_2, CO, CH_4 and CH_2O. The first observations of CH_4 from TROPOMI came from radiance measurements of the shortwave infrared band around 2.3 [μm], and was published in 2018 (Hu et al., 2018). TROPOMI provides daily global coverage with spatial resolution down to 7×7 [km] for CH_4. In the study of Zhang et al. (2020), observations from TROPOMI was used to quantify methane emissions from the Permian basin in the U.S., a massive oil-producing region.

1.4.2 Regional

On the regional level, one of the leading European greenhouse gas monitoring networks is the Integrated Carbon Observation System (ICOS), which consists of about 140 monitoring stations spread out across 12 European nations (ICOS, 2020). The ICOS stations perform observations of atmospheric greenhouse gases and carbon flux measurements between the ocean, atmosphere, and land-surface. The north American equivalent of ICOS is the National Oceanic and Atmospheric Administration (NOAA) Global Greenhouse Gas Reference Network, which also provides observations and studies of greenhouse gases, predominantly in the United States. This includes tall tower measurements, surface sam-

ples, and aircraft measurements. Another regional EU-funded project is the MEthane goes MObile - MEasurements and MOdelling ($MEMO^2$) network, which focuses on local and regional emissions of CH_4. The $MEMO^2$ framework consists of more than 20 collaborators from 7 different counties. $MEMO^2$'s goal is to develop and apply innovative experimental and modeling tools based on state-of-the-art techniques, identify and quantify methane emissions from European sources, and use these updated emissions to improve the estimates at the European scale (Walter et al., 2020).

Another initiative that focuses on regional and local emissions is the Carbon Dioxide and Methane Mission (CoMet). The overall goal of CoMet is to obtain independent observations of GHGs by developing and evaluating new methodologies that can also be used for the validation of satellite measurements (Fiehn et al., 2020). Here, airborne in-situ measurements, mobile ground-based measurements, and active and passive remote sensing measurements are combined to quantify CO_2 and CH_4 emissions. The CoMet 1.0 campaign focused on quantifying the regional emissions from the Upper Silesian Coal Basin (USCB) in Poland's southern province, Silesia (Nickl et al., 2020).

The use of a tower to obtain greenhouse gas measurements, such as those provided in the ICOS network, is a common technique that has been around for a long time. In the study of Werner et al. (2003), CH_4 measurements over a mixed temperate/boreal lowland, and wetland forest, were obtained from a 447 [m] tall tower over two years. These measurements were used to quantify the regional-scale CH_4 exchange. A detailed evaluation of CO_2, CO, and CH_4 measurements from NOAA/Earth System Research Laboratory(ESRL) tall towers was performed by Andrews et al. (2014). Another example is the study from Satar et al. (2016). Here, continuous tall-tower measurements of CO_2, CH_4, and CO were made over two years.

Aircraft measurements are also commonly used in regional studies of CH_4. Among many examples, Karion et al. (2013) obtained measurements of methane from an aircraft flown over a natural gas field in the western united states and quantified its emissions using a mass balance approach. Miller et al. (2013) estimated anthropogenic methane sources in the United States between 2007 and 2008, using surface measurements, tower measurements, and aircraft measurements in combination with an atmospheric transport model. In the study of Sweeney et al. (2015), ten years of NOAA/ESRL CO_2 aircraft measurements was used to observe seasonal climatology. This study also considered other trace gases, such as CO, CH_4, N_2O, and SF_6. A Twin Otter research aircraft was used by Peischl et al. (2016, 2018) to measure in-situ CH_4 and ethane (C_2H_6) concentrations, and quantify methane fluxes from oil and natural gas production sites in North Dakota. Krautwurst et al. (2017) used airborne remote sensing and in-situ measurements to estimate the CH_4 emissions from a California landfill. Estimates of CH_4 emissions over a major U.S. shale gas basin were made by Schwietzke et al. (2017) using a Mooney Ovation aircraft equipped with a CRDS methane analyzer. Hartery et al. (2018) used aircraft measurements over Alaska to estimate the regional CH_4 flux, while Gasbarra et al. (2019) used aircraft data and measurements of CH_4 to locate and quantify emissions from four co-located landfills near Naples, Italy. Hannun et al. (2020) combined tower measurements with aircraft measurements and estimated the spatial heterogeneity in CO_2 and CH_4 over the mid-Atlantic region.

1.4.3 Local

The local scale studies are smaller in scale, such as studies on single power plant facilities, point source emissions from a coal mines, or small area sources such as that of an individual farm or natural gas storage facility. Techniques of measuring local-scale methane consist of various tools, among them mobile measurement using vans or automobiles. Atherton et al. (2017) used mobile van measurements fitted with a Los Gatos Research (LGR) CO_2 and CH_4 analyzer to measure emissions from natural gas developments in northeastern British Columbia, Canada. Caulton et al. (2018) used an inverse Gaussian approach together with mobile van-based observations of methane to quantify methane emission uncertainties from oil- and gas wells in Pennsylvania, U.S. In the study of Kumar et al. (2020), a mobile van was used to obtain measurements of CO_2 and CH_4 from point sources. These measurements were processed using a Gaussian plume dispersion model to invert the CH_4 and CH_2 flux and the location of the source. Maazallahi et al. (2020) used a mobile van fitted with Cavity Ring-Down Spectrometry models G2301 and G4302 to measure methane concentrations, CO_2, C_2H_6, and isotopic composition through the streets of Utrecht, NL, and Hamburg, DE.

Mobile measurements of CH_4 using unmanned aerial vehicles have, in recent years, become more common. Nathan et al. (2015) used a fixed-wing model aircraft to measure and quantify methane emission variability from a compressor station in the Barnett Shale, U.S. In the study of Allen et al. (2019), they used a UAV system to estimate the methane flux from two landfill sites in England using proxy measurements of CO_2 concentration and wind data. Shah et al. (2020) used a tethered UAV to sample a point source methane plume near the source and estimating the emitted methane flux using a near field Gaussian mass balance approach. Vinkovic et al. (2021) quantified the CH_4 flux from a dairy cow farm in the eastern part of Groningen, NL, using a mass balance approach on sampled air downwind the farm. The air was sampled using an active AirCore system attached to a UAV and was analyzed for CH_4 and N_2O mole fractions.

Open-path measurements and aircraft measurements are also powerful techniques that can also be used on local-scale studies. Arndt et al. (2018) used both of these, as well as mobile van measurements, to estimate the short-term CH_4 emissions from two dairy farms in California, U.S. In the study of Daube et al. (2019) a tracer flux ratio method was used in combination with aircraft measurements of CH_4 to quantify emissions from two dairy farms in central California, U.S.

1.5 Unmanned aerial vehicle-based measurements

The use of unmanned aerial vehicles (UAVs), also often referred to as unmanned aerial systems (UAS) or drones, have in recent years become an important tool for greenhouse gas measurements. They are cheap to obtain, maintain, and to pilot compared to an aircraft, and especially for smaller UAVs of a few kilos, it is often easier to obtain permits for flying. Smaller UAVs also require no additional certification to operate if custom modifications are needed (Kunz et al., 2020). On top of this, their maneuverability makes them very suitable to use in small-scale studies where space is limited and areas are hard to

access. They can provide vertical and horizontal profiles, and can fly closer to the ground and certain sources compared to crewed aircraft. UAVs are capable of autonomous flying from take-off to landing, and pre-flight programming of flights trajectories, which means smaller UAVs can be flown with higher accuracy and less workload for the pilot (Villa et al., 2016). However, the payload capacity of smaller UAVs is often limited in how large the instrumentation can be, and how heavy. It is therefore of vital importance to develop smaller and lightweight instrumentation that can be attached to a UAV, to perform accurate trace gas sampling while benefiting from the UAVs mobility and versatility.

The use of UAVs in GHG measurements can broadly be separated into three main categories, which are 1) UAV studies that perform in-situ, or direct measurements in the atmosphere, using some sort of mounted sensor or analyzer that yields immediate results. Examples of studies that utilize this form of UAV in-situ sampling are the studies by Berman et al. (2012), Khan et al. (2012), Nathan et al. (2015), Brady et al. (2016), Kunz et al. (2018), Golston et al. (2017), Kunz et al. (2020), Martinez et al. (2020), and Tuzson et al. (2020). 2) UAVs that are tethered, which means that a tube is attached to the UAV in one end, and to a ground-based analyzer in the other. This allows the air to be sampled at the UAVs location, and dragged through the tube to be directly analyzed on the ground, however, the distance the drone can fly is limited by the length of the tube. Examples of studies that perform tethered UAV sampling are those by Turnbull et al. (2014), Brosy et al. (2017), Wolf et al. (2017), Allen et al. (2019), Shah et al. (2019), and Shah et al. (2020). 3) UAVs that perform on-board sampling of air, meaning that they take and store an air sample while the UAV is flying, that can later be analyzer on the ground. Examples of UAV on-board sampling studies include those of Lowry et al. (2015), Brownlow et al. (2016), Chang et al. (2016), Greatwood et al. (2017), and Andersen et al. (2018).

The use of UAVs is a fairly new addition to the greenhouse gas measurement arsenal, and there are numerous studies working on the further development of smaller and more accurate sensors and systems capable of measuring atmospheric trace gases using both large, and smaller commercial UAVs.

A fixed-wing model aircraft equipped with a 3.1 [kg] open-path methane sensor was used by Nathan et al. (2015) to characterize methane mission variability from a compressor station in the Barnett Shale, U.S. The methane sensor performed high-frequency (10 [Hz]) measurements of CH_4 with a precision of 0.1 [ppm]. Brady et al. (2016) used a small multi-copter equipped with a 500 [g] payload to perform high-spatial-resolution (1 [m]), near-surface (0 - 100 [m]) vertical profiles of CO_2. The payload consisted of a two-channel aerosol optical particle counter and a low-cost CO_2 sensor system capable of measuring in the range of 0 - 10000 [ppm] with a sensitivity of 30 [ppm] ± 3 [%] of the measurement reading. Kunz et al. (2018) developed a CO_2 measurement system that could be carried by any lightweight UAV with a payload capacity that exceeds 1.2 [kg]. The measurement error for atmospheric CO_2 was 1.2 [ppm]. Greatwood et al. (2017) flew small unmanned multi-rotors and sampled air using tedlar bag samples that was later analyzed for methane concentration and isotopic composition using a cavity ring-down spectrometer. The tedlar bag sampling system was below 0.5 [kg]. Allen et al. (2019) developed a sampling method to infer methane fluxes using CO_2 proxy measurements, along with UAV recorded wind

measurements. One fixed-wing UAV was used for in-situ CO_2, while a 100 [m] tethered rotary UAV was used to obtain vertical profiles of both CO_2 and CH_4 using a Los Gatos Research Ultra-portable Greenhouse Gas Analyzer (LGR-UGGA). For two separate days, they derived flux estimates using a mass balance approach of 0.140 [kg s^{-1}] (±61 [%] at 1σ), and 0.050 [kg s^{-1}] (±54 [%] at 1σ), respectively. Martinez et al. (2020) developed a open-path Cavity Ring-Down Spectrometer (CRDS) sensor for in-situ methane sampling using small UAV systems, below 25 [kg]. The spectrometer payload weighed 4.1 [kg] and had a methane sensitivity $\sim<$ 30 [ppb]. Tuzson et al. (2020) developed a compact Quantum Cascade Laser (QCL) spectrometer capable of high sensitivity and time resolution (1 [Hz]) measurements of CH_4 with a precision of 1.1 [ppb], lowered to 0.1 [ppb] using a 100 [s] averaging window. The total payload weight was 2.1 [kg], capable of being lifted by a large number of commercial UAVs.

1.5.1 Active AirCore System

This section will briefly introduce the active AirCore System which is utilized throughout this thesis. A detailed description of its components, performance, and use is found in chapter 2. The active AirCore system is an air sampling tool for greenhouse gases that utilizes the mobility and versatility of an unmanned aerial system. An illustration along with an actual image of the active AirCore system is shown in figure (1.4). It is comprised of a 50 [m] long stainless steel tube that is capable of storing the sampled air without great loss of the spatial resolution. Air is pulled from the inlet through the tube by a small pump that works together with a small pinhole orifice to create critical flow. This means that the flowrate of the sampled air remains constant with respect to ambient pressure, which is measured by a datalogger, along with temperature and humidity. The total size of the system is roughly as large as a shoe-box and weighs in at around 1 [kg], which makes it small and light enough to be carried by most commercial UAVs. Throughout the work of this thesis, the UAV model DJI Inspire 1 Pro was used to carry the active AirCore system, as shown in the lower right picture of figure (1.4).

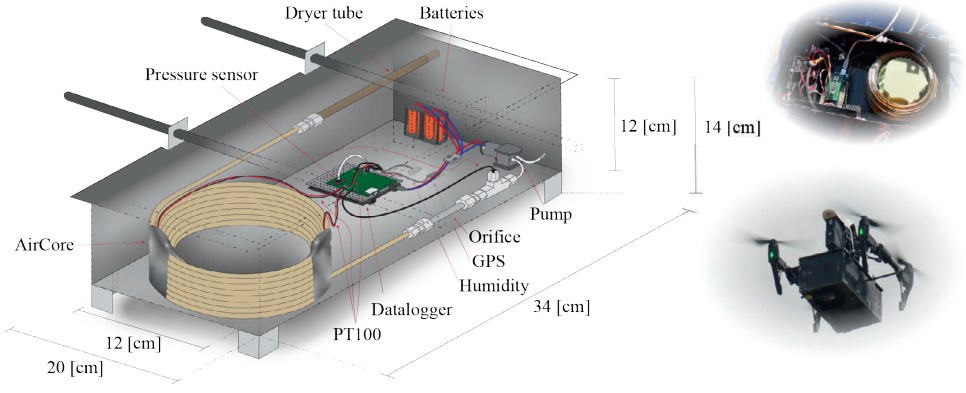

Figure 1.4. shows a schematic design of the active AirCore system and its components. Pictures of the active AirCore system (north-east), and of the system attached to the DJI Inspire 1 Pro in-flight are also shown.

1.6 Dispersion of CH_4 plumes

One of the focuses of this thesis will be methane quantification from point sources. These are sources of pollution where the emanating flux is from a small area, such as a chimney or ventilation shaft. One of the more common air pollution distribution models used to describe point source emission is the Gaussian plume model, which describes the three-dimensional mole-fraction map generated by a point source under constant meteorological conditions (Zannetti, 1990). The model, as described by Lagzi et al. (2013), follows:

$$C(x,y,z) = \frac{Q}{2\pi\ \sigma_y\ \sigma_z\ u}\ e^{\left(-\frac{1}{2}\left(\frac{y}{\sigma_y}\right)^2\right)}\left[e^{\left(-\frac{1}{2}\left(\frac{h-z}{\sigma_z}\right)^2\right)} + e^{\left(-\frac{1}{2}\left(\frac{h+z}{\sigma_z}\right)^2\right)}\right] \tag{1.2}$$

where the concentration C (in [kg m^{-3}]) is given at position x, y, and z (see figure (1.5)). The units of x, y, and z are given in [m]. The emission rate Q is given in [kg/s], the wind speed u in [m/s], and the stack height h is given in [m]. The parameters σ_y and σ_z describe the mixing of the pollutants, or turbulence, in the horizontal- and vertical direction, respectively, and have units of [m]. To arrive at the equation (1.2), one has to assume steady-state conditions and that the mass of the pollutant is conserved. This implies that the pollutant experiences no radioactive decay, no chemical transformation, and no deposition (Holmes and Morawska, 2006). Meteorological conditions are also assumed to remain constant from source to receptor. However, this is not the case in practice, as a plume's characteristics can change over time due to their dependence on changing emissions and meteorological conditions (Bandyopadhyay, 2009). An illustration of the Gaussian distribution model is shown in figure (1.5).

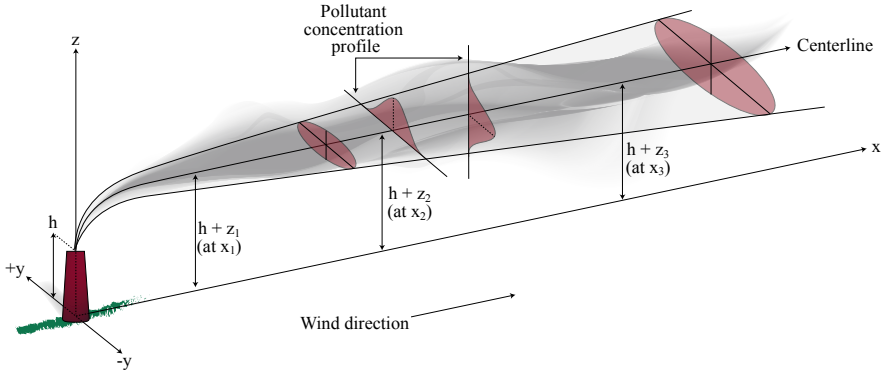

Figure 1.5. shows an illustration of a buoyant Gaussian air pollutant dispersion plume. This figure is a re-illustration of the figure originally published by Leelőssy et al. (2014).

Turbulent mixing in the atmosphere is driven by wind shear and buoyancy, and there have been several methodologies that explore how the dispersion coefficients, σ_y and σ_z, are determined. However, these methodologies share a common weakness, which is the inability to calculate short-term time averages (Hoinaski et al., 2016). This is discussed more in section (1.6.3). One of these commonly used methodologies is the method developed by Pasquill (1961). He defined six separate stability classes, ranging

from a very unstable boundary layer (Stability class A) to a stable boundary layer (F). Turner (1970) revised this, and this methodology is now known as the Pasquill-Gifford method (see table (1.1)). The stability classes are based on wind speed, cloud coverage, and solar radiance.

Table 1.1. shows Pasquill-Gifford stability classes (Pasquill, 1961; Turner, 1970): (**A**): Very unstable, (**B**): Unstable, (**C**): Slightly unstable, (**D**): Neutral, (**E**): Slightly stable, and (**F**): Stable boundary layer.

Surface wind speed [m/s]	Incoming solar radiation [W m^{-2}]			Nighttime conditions	
	Strong (> 700)	Moderate (350 - 700)	Slight (< 350)	Thin overcast or > 50 [%] low cloud	≤ 50 [%] cloudiness
<2	A	A - B	B	E	F
2 - 3	A - B	B	C	E	F
3 - 5	B	B - C	C	D	E
5 - 6	C	C - D	D	D	D
>6	C	D	D	D	D

1.6.1 Plume rise

To calculate the plume rise, buoyancy has to be considered. In equation (1.2), the plume's effective height at a distance x downwind of the plume is a product of the stack height, and the plume rise Δh. A common way of calculating the plume rise is by using the Briggs equations (Briggs, 1969, 1972), shown in figure (1.6). The Briggs buoyancy flux parameter (in $[m^4 s^{-3}]$) is given as:

$$F = g\ v_s\ d_s^2 \left(\frac{\Delta T}{4T_s}\right) \tag{1.3}$$

where g is the gravitational acceleration (in [m/s^2]), v_s is the stack gas exit velocity (in [m/s]), d_s is the inside stack top diameter (in [m]), $\Delta T = T_s - T_a$, with T_s being the stack gas temperature (in [K]), and T_a the ambient air temperature (in [K]). Following the logic diagram presented by Briggs (see figure (1.6)), the rise of a buoyant plume can be estimated.

For stable situations (Stability classes E and F), the stability parameter, s, is required to estimate the plume rise. This includes the atmospheric lapse rate, and is calculated as follows:

$$s = g \frac{\partial\theta/\partial z}{T_a} \tag{1.4}$$

where $\partial\theta/\partial z$ is the atmospheric lapse rate (in [K/m]). We can now put into perspective by following the Briggs equations: given stability class D with lapse rate of -0.005 [K/m] and a hypothetical point source with a diameter of 4 [m], exit velocity of 2 [m/s], stack

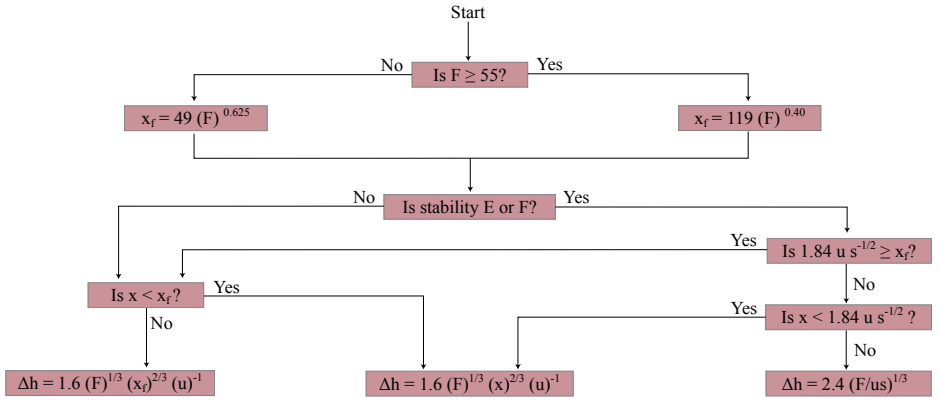

Figure 1.6. shows a logic diagram for Briggs' equations to calculate the rise of a buoyant plume, where Δh is the plume rise (in $[\mathrm{m}]$), F is the Buoyancy factor (in $\left[\mathrm{m^4 s^{-3}}\right]$), x is the downwind distance form the source (in $[\mathrm{m}]$), x_f is the downwind distance from the source to the point of maximum plume rise (in $[\mathrm{m}]$), u is the windspeed at the stack height (in $\left[\mathrm{m/s}\right]$), and finally, s is the stability parameter (in $\left[\mathrm{s^{-2}}\right]$).

temperature of 298.15 [K] (25 [°C]) on a day with ambient temperature of 273.15 [K] (0 [°C]) and wind speed of 2 [m/s], the plume rise 100 [m] downwind is 33 [m]. Similarly, stability class E with a lapse rate of 0.015 [K/m] and stability class F with a lapse rate of 0.020 [K/m] would have plume rise of 45 [m] and 41 [m] respectively, at a downwind distance of 50 [m].

1.6.2 Vertical and horizontal dispersion parameters

The Pasquill-Gifford method has the advantage that the turbulence parameters can be estimated directly from simple meteorological measurements. This method's drawback is that the accuracy of these pre-defined stability classes is often low compared to that of more sophisticated models. The Pasquill-Gifford measurements were taken in open, rural surroundings. Due to the origin of these measurements, the methodology is not well equipped for urban areas and is mostly limited to rural settings (Abdel-Rahman, 2008).

Other methods to estimate turbulence include the Richardson number (Galperin et al., 2007) and the Monin-Obukhov theory (Monin and Obukhov, 1954). However, these will not be discussed here. A commonly used way of estimating the dispersion parameters is by using equations (1.5) and (1.6):

$$\sigma_y = \frac{r\ x}{\left(1 + \frac{x}{a}\right)^p} \qquad (1.5) \qquad\qquad \sigma_z = \frac{s\ x}{\left(1 + \frac{x}{a}\right)^q} \qquad (1.6)$$

where x is the downwind distance (in $[\mathrm{m}]$). These equations are analytical expressions based on the Pasquill-Gifford curves and use the vertical temperature gradient ($\Delta \mathrm{T}/\Delta \mathrm{Z}$) to determine the dispersion parameters (Green et al., 1980; Sharan et al., 1995). The values for the stability class dependent parameters a, s, q, r, and p are given in table (1.2). It is important to note, however, that the Pasquill-Gifford coefficients were made over periods of 10 - 20 minutes and are therefore only applicable to these time-frames. This is elaborated on in the following section.

Table 1.2. shows the values for the Pasquill-Gifford parameters (Green et al., 1980; Sharan et al., 1995) for each stability class, used in the calculation of the dispersion parameters (See eq. (1.5) and (1.6)), along with the vertical temperature gradient at each stability class.

Class	a [m]	s [m/m]	q	r [m/m]	p	$\Delta T/\Delta Z$ [K/100 m]
A	927	0.1020	-1.918	0.250	0.189	< -1.9
B	370	0.0962	-0.101	0.202	0.162	-1.9 to -1.7
C	283	0.0722	0.102	0.134	0.134	-1.7 to -1.5
D	707	0.0472	0.465	0.079	0.135	-1.5 to -0.5
E	1070	0.0335	0.624	0.057	0.137	-0.5 to 1.5
F	1170	0.0220	0.700	0.037	0.134	> 1.5

1.6.3 Limitations

It is important to note that the instantaneous sampling of a Gaussian distribution plume will not provide an accurate representation of the dispersion. The general rule in many atmospheric dispersion handbooks and manuals and many literary studies is that averaged concentrations over 10 minutes provide a satisfactory result (Stockie, 2011). The time interval should be long enough for the plume emissions to reach a steady-state distribution, but short enough to capture the largest changes in the wind speed. The concept of time-averaging is illustrated in figures (1.7) **a** and **b**.

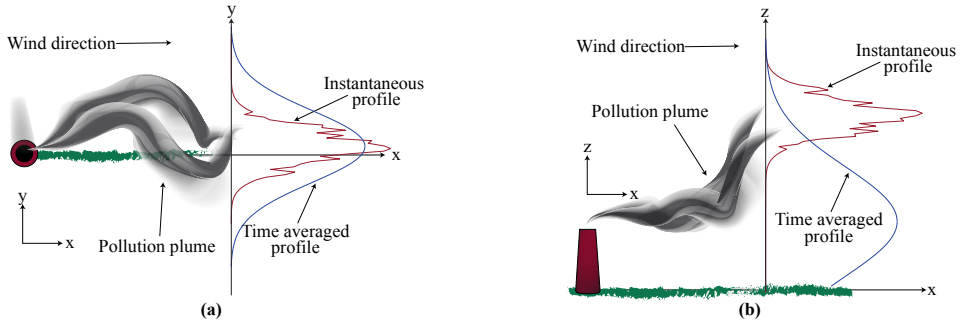

Figure 1.7. Illustration showing the difference between an instantaneous concentration profile (red curves), and that of a time-averaged concentration profile (blue curves). Figure (**a**) is a top-down view, while (**b**) is a side perspective.

Due to concentration levels reaching infinity near the source, the Gaussian dispersion models are only accepted to calculate concentrations at distances > 100 [m] away from the source (Briggs, 1973). When using Gaussian distribution models to invert fluxes, it is crucial for the pollutant sampling to take place at distances exceeding 100 [m] from the source. The model performs poorly at low wind speeds due to the inverse wind speed dependence of the steady-state plume equation. While sampling, consistent wind direction, and more substantial wind speeds are therefore advantageous. To obtain the

optimal results, sampling is required not to be instantaneous and average 10 minutes.

The work presented in this thesis, mole fractions of CH_4 will be used to constrain the shape of the Gaussian model (eq. (1.2)). In practice, this means that the output of the Gaussian dispersion model is fitted to the data using a standard square error optimization, which optimizes the parameters for plume rise, dispersion parameters, and emission rate directly, regardless of stability class.

1.7 Objectives and thesis outlook

Atmospheric GHG measurements are essential to help constrain the global methane budget. Mobile UAVs provide the possibility to measure GHGs in places that are hard to reach, with both vertical and horizontal profiles. **The goal of this Ph.D. is to develop a unmanned aerial vehicle-based system for atmospheric measurements of greenhouse gases and employ the system to quantify local to regional emissions of methane**. This thesis presents the development, testing, and use of an active AirCore sampling system in combination with a commercial quad-copter UAV (DJI Inspire 1 Pro) to sample and quantify emissions of methane and other atmospheric trace gases.

First, a system to accurately sample and preserve an air sample along a flown trajectory without significant spatial resolution loss was developed. This instrument is called an active AirCore system and works by pulling air through a 50 [m] stainless steel tube at a constant flowrate, maintained by ensuring critical flow through a small pinhole orifice. Laboratory- and field testing are performed to demonstrate the versatility and accuracy of the technique. This work is presented in **Chapter 2**.

The following chapter focuses on utilizing the newly developed mobile active AirCore system and developing a methane point source quantification technique. Fifteen flights and measurements were taken from a single anthracite coal-mine ventilation shaft in the Polish coal-mining region of Silesia. These profiles are used to quantify methane and carbon dioxide emissions fluxes by combining the profiles with a mass balance- and inverse Gaussian-approach. This work is presented in **Chapter 3**.

The development of a methane point source quantification technique using the mobile active AirCore system was then used to further expand on the regional emissions emanating from the Upper Silesia Coal Basin (USCB). We performed 59 flights and measured emitted methane concentrations from 5 different coal mining shafts, spread out across the USCB. Tedlar bag samples containing an integrated methane concentration for each flight was also obtained and analyzed for δ^{13}C-CH_4 and δ^{2}H-CH_4 to acquire the isotopic signature for the methane emissions. We estimate the regional emissions and compare this with inventories and other scientific studies. This work is presented in **Chapter 4**.

The findings are synthesized and discussed in **Chapter 5**, and finally, the thesis ends with a summary.